

# Blazar sequence – an artefact of Doppler boosting

E. Nieppola<sup>1</sup>, E. Valtaoja<sup>2,3</sup>, M. Tornikoski<sup>1</sup>, T. Hovatta<sup>1</sup>, M. Kotiranta<sup>1</sup>

<sup>1</sup> Metsähovi Radio Observatory, TKK, Helsinki University of Technology, Metsähovintie 114, FIN-02540 Kylmälä, Finland  
e-mail: elina.nieppola@tkk.fi

<sup>2</sup> Tuorla Observatory, Väisäläntie 20, 21500 Piikkiö, Finland

<sup>3</sup> Dept. of Physical Sciences, University of Turku, 20100 Turku, Finland

Received / Accepted

## ABSTRACT

**Context.** The blazar sequence is a scenario in which the bolometric luminosity of the blazar governs the appearance of its spectral energy distribution. The most prominent result is the significant negative correlation between the synchrotron peak frequencies and the synchrotron peak luminosities of the blazar population.

**Aims.** Observational studies of the blazar sequence have, in general, neglected the effect of Doppler boosting. We study the dependence of both the synchrotron peak frequency and luminosity with Doppler-corrected quantities.

**Methods.** We determine the spectral energy distributions of 135 radio-bright AGN and find the best-fit parabolic function for the distribution to quantify their synchrotron emission. The corresponding measurements of synchrotron peak luminosities and frequencies are Doppler-corrected with a new set of Doppler factors calculated from variability data. The relevant correlations for the blazar sequence are determined for these intrinsic quantities.

**Results.** The Doppler factor depends strongly on the synchrotron peak frequency, the lower energy sources being more boosted. Applying the Doppler correction to the peak frequencies and luminosities annuls the negative correlation between the two quantities, which becomes *positive*. For BL Lacertae objects, the positive correlation is particularly strong.

**Conclusions.** The blazar sequence, when defined as the anticorrelation between the peak frequency and luminosity of the synchrotron component of the spectral energy distribution, disappears when the intrinsic, Doppler-corrected values are used. It is an observational phenomenon created by variable Doppler boosting across the synchrotron peak frequency range.

**Key words.** galaxies: active – BL Lacertae objects: general – quasars: general – radiation mechanisms: non-thermal

## 1. Introduction

The most powerful active galactic nuclei (AGN) are active emitters at almost all frequencies and exhibit both strong flaring and typically high polarization. These sources are referred to, in general, as blazars. The source of their power is a supermassive black hole embedded in the host galaxy, which generates a massive accretion process. The bulk of the continuum radiation from these sources does not, however, originate in the nucleus, but in two jets that emerge symmetrically from the core. A tell-tale sign of the presence of jets is strong radio continuum, which is believed to be produced via synchrotron process by relativistic electrons spiralling in the magnetic field of the jet. This synchrotron radiation can be seen in the blazar spectral energy distribution (SED) as a bump at radio to X-ray frequencies in the  $\log \nu - \log(\nu F_\nu)$ -representation. It is followed by another bump, which is often attributed to the inverse Compton process.

The shape and position of the synchrotron SED component in the  $\log(\nu F_\nu)$  versus  $\log \nu$  coordinate system and the mechanisms that control its properties have been discussed for a number of years. It was first suggested by Padovani & Giommi (1995) that the peak of the synchrotron component can occur at any frequency from radio to soft X-rays, producing detectable differences in the source properties, such as broad band spectral indices. The position of the synchrotron component peak on the  $\log \nu$ -axis, the synchrotron peak frequency  $\nu_p$ , was linked to the intrinsic synchrotron peak luminosity,  $\nu_p L_{\nu,p}$ , by Fossati et al. (1998) and Ghisellini et al. (1998). They proposed

that there was a negative correlation between the two quantities, that is sources with their peak frequency in the radio band would be more luminous than those that had their peak in the X-ray band. This correlation would be created by decreasing intrinsic power and decreasing cooling effects, caused by external radiation field, as the synchrotron peak moves from low to high energies (Ghisellini et al. 1998). The blazar luminosity sequence has been studied by many authors (e.g., Padovani et al. 2003; Caccianiga & Marchã 2004; Antón & Browne 2005, for a concise review of the present status of the blazar sequence, see Padovani (2007)). Lately, evidence against it has been mounting; as the number of blazars known has increased, it has been found that the previously-observed correlation does not describe the newer data sets. Ghisellini & Tavecchio (2008) attempted to explain these outliers using a revised theoretical blazar sequence, which related the SED shape to the mass of the central black hole and its accretion rate. This new scheme reduced the tightness of the correlation between the peak frequency and luminosity, allowing the presence of high-luminosity high- $\nu_p$  objects, and even predicting the existence of low-power low- $\nu_p$  objects. However, the negative trend between the two quantities was, in general, expected to hold. In Nieppola et al. (2006, hereafter Paper I) the synchrotron peak frequencies of more than 300 BL Lacertae objects (BL Lacs, BLOs) were determined and used to plot the  $\nu_p L_{\nu,p}$  versus  $\nu_p$ -correlation. No significant anticorrelations could be found using this extensive sample, which included many high-energy sources.

One important matter overlooked in these observational studies of the blazar sequence was the effect of Doppler boosting. When the source of the continuum radiation (i.e., the shocked plasma in the jet) is moving towards us, the observed radiation is blueshifted and enhanced significantly (Blandford & Königl 1979). The amount of Doppler boosting depends on the viewing angle of the jet,  $\theta$ , and the Lorentz factor  $\gamma$ . It is therefore clear that the Doppler factor  $D$  is by no means similar for all AGN, or even for all blazars, which implies that it can significantly effect the appearance of the blazar sequence. In the original blazar sequence papers (Fossati et al. 1998; Ghisellini et al. 1998) and in theoretical work (Ghisellini & Tavecchio 2008), the Doppler factor was assumed to be constant irrespective of the peak frequency  $\nu_p$ . In this paper, we demonstrate that this assumption is inaccurate. We examine the  $\nu_p$  versus  $\nu_p L_{\nu,p}$  -correlation for a complete sample of AGN using Doppler-corrected values based on new estimates of Doppler-boosting factors (Hovatta et al. 2008, in preparation). In this way, we are able to determine if there is any pattern in the intrinsic, true properties of the sources.

The paper is organized as follows: in Sect. 2 we present the source data that we study, and in Sect. 3 we describe the methods of acquiring the data. In Sect. 4, we present the results, and finish with a discussion and conclusions in Sects. 5 and 6, respectively. Henceforth, all luminosities are frequency dependent. For clarity, we denote luminosities simply with  $L$  instead of  $L_\nu$ , and use the subscript  $p$  to denote peak frequency and luminosity of the synchrotron component determined directly from the SED. Throughout this paper, we assume  $H_0 = 65 \text{ km s}^{-1} \text{ Mpc}^{-1}$  and  $\Omega_0 = 1$ .

## 2. Sample

We study sources selected from the Metsähovi Radio Observatory source list, which meet one or both of the following criteria:

1. The source has a declination of  $\geq 0$  deg and the highest observed flux exceeds 1.2 Jy at 37 GHz.
2. The source has a Doppler factor determined by either Lähteenmäki & Valtaoja (1999) or Hovatta et al. 2008 (in preparation).

Sources meeting the first criterion comprise a complete northern flux-limited radio-loud AGN sample; they constitute a large majority of the entire sample, 113 sources out of 135. The remaining sources are radio loud as well, but do not reach the flux limit of 1.2 Jy, or are southern sources. They are included because they have well sampled radio flares at 22 or 37 GHz, allowing a reliable determination of the Doppler factor from variability data. The full sample consists of 34 highly polarized quasars (HPQ), 33 quasars of low polarization (LPQ), 31 BL Lacertae objects (BLO), 26 quasars with no polarization data (QSO), 9 radio galaxies (GAL), and 2 unclassified objects. HPQs have a measured polarization of  $\geq 3$  % in the literature and LPQs have a polarization of  $< 3$  %. BLOs are included in Véron-Cetty & Véron (2000), or defined as such in the literature. GALs are radio galaxies of varying properties, which all are non-quasars.

The full sample is listed in Table 1. Columns (1) and (2) provide alternative names for the source and Cols. (3) and (4) indicate the right ascension and declination, respectively. Column (5) indicates whether the source belongs to the 1.2 Jy complete sample. Column (6) provides the classification of the source, our

measurement of the synchrotron peak frequency (see Sect. 3.1) is listed in Col. (7), and Col. (8) gives the redshift of the source. Finally, Col. (9) indicates the sources that belong to the blazar sample discussed in Sect. 4.2.

## 3. Methods

### 3.1. Spectral energy distributions

The spectral energy distributions of our selected sample were determined in a similar manner to those of Paper I. A significant quantity of multi-frequency data were collected from various sources, including the CATS database<sup>1</sup> of the Special Astrophysical Observatory (Verkhodanov et al. 2005) and the NED database<sup>2</sup> at IPAC. Most sources have a low-energy synchrotron peak and we were able to find a substantial amount of radio data. The majority of the high frequency radio data were acquired from Metsähovi Radio Observatory (Salonen et al. 1987; Teräsraanta et al. 1992, 1998, 2004, 2005; Nieppola et al. 2007, and some unpublished data). IR-data from IRAS or 2MASS catalogues, or from ISO (Padovani et al. 2006) were also available for most sources in the aforementioned databases. In addition to X-ray datapoints found in the databases, we used 1 keV monochromatic fluxes from Donato et al. (2001).

The SEDs were plotted in  $\log \nu - \log (\nu F_\nu)$  parameter space and are presented in Fig. 5 (published electronically). The synchrotron components of the SEDs were fitted by a simple parabolic function

$$\log (\nu F_\nu) = A (\log \nu)^2 + B (\log \nu) + C, \quad (1)$$

where A, B, and C are constants. Thus, the synchrotron peak frequency is given by

$$\log \nu_p = \frac{-B}{2A}. \quad (2)$$

With knowledge of  $\nu_p$ , we can calculate the peak flux density,  $\nu_p F_{\nu,p}$ , using Eq. 1. The peak frequencies obtained in this work are listed in Col. (7) of Table 1.

In Fig. 5, datapoints included in the fitting are marked by filled circles and other datapoints are marked by open rectangles. For the sake of consistency, we excluded datapoints below 1 GHz from all fits. Below that frequency, the SEDs often feature an additional flattening originating from an extended component; we therefore applied a cutoff to avoid any contamination in the jet synchrotron fit. The synchrotron peak frequency could be determined for all but two sources: 1019+222 and 1845+797. These objects have peculiar spectral shapes which could not be fitted accurately using a parabolic function.

Our sample consists of radio-bright AGN, which typically have a relatively low synchrotron peak frequency. Thus, in most SED fits, we did not include the X-ray datapoints in the synchrotron component. Our decision was made based on a careful visual inspection and the X-ray spectral index when possible. In some powerful BLOs, such as 0219+428 and 1652+398, the synchrotron component extends to the X-ray domain. In the case of 0735+178, the X-ray data are also included in the synchrotron component in the interest of constraining the fit and providing a more accurate estimate of  $\nu_p$ . The X-ray indices of the SEDs are taken from Donato et al. (2001). For clarity, they are plotted in the energy range 1 - 10 keV and are normalized with respect to the 1 keV monochromatic flux listed in Donato et al. (2001).

<sup>1</sup> <http://cats.sao.ru>

<sup>2</sup> <http://nedwww.ipac.caltech.edu/>

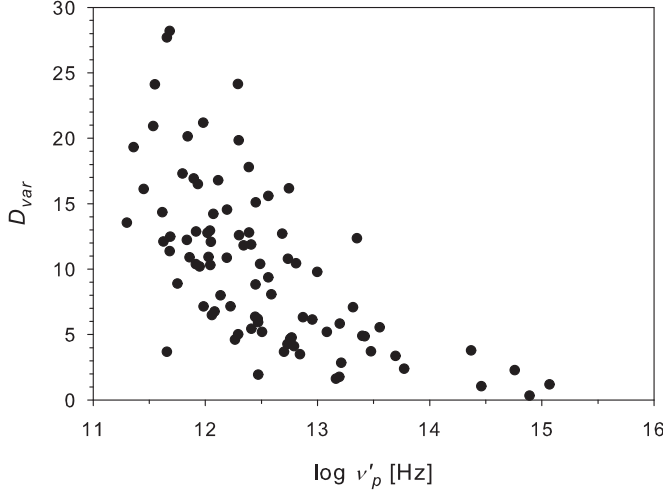


**Fig. 1.** The variability Doppler factors  $D_{var}$  plotted against the synchrotron peak frequency. The  $\nu'_p$ -values are  $D$ -corrected.

There was one case, namely 0430+052, where the synchrotron peak was exceptionally well sampled, but the parabolic function did not fit the data very well. To avoid using an obviously flawed  $\nu_p$ , we assigned a new value using the true peak defined by the highest point of the synchrotron bump. Thus, we obtained  $\log \nu_p = 13.95$ , instead of  $\log \nu_p = 15.94$  provided by the fit. The same approach was considered for 0316+413, but the two methods yielded almost identical results. In the analyses, we used the fit value  $\log \nu_p = 14.40$ .

### 3.2. Doppler factors

To calculate the de-boosted, intrinsic values of  $\nu_p$  and  $\nu_p L_p$ , we need to calculate the Doppler boosting factors  $D$ . These have been calculated in the past using several methods (e.g. Ghisellini et al. 1993; Güijosa & Daly 1996; Guerra & Daly 1997; Lähteenmäki & Valtaoja 1999; Jorstad et al. 2005; Wu et al. 2007). In this work, we use the  $D_{var}$ -values of Hovatta et al. 2008 (in preparation), which have been determined from total flux density variability data in the same manner as in Lähteenmäki & Valtaoja (1999). The flux curves from long-term monitoring at 22 and 37 GHz at Metsähovi Radio Observatory are decomposed into exponential flares. The exponential fit provides the necessary parameters for the calculation of the variability brightness temperature  $T_{b,var}$ ; comparing  $T_{b,var}$  with the equipartition value  $T_{eq}$  then provides the amount of boosting. Both Lähteenmäki & Valtaoja (1999) and Hovatta et al. (2008) used the equipartition value of  $5 \times 10^{10}$  K proposed by Readhead (1994).

We were able to derive  $D_{var}$  for 89 sources in our sample. The remainder of the sample had to be excluded from the study of intrinsic properties. The values of  $D_{var}$  and a detailed explanation of their determination will be published in a future paper (Hovatta et al. 2008).

## 4. Results

### 4.1. The dependence of $D_{var}$ and $\nu_p$

For studies of the blazar sequence, the crucial question is whether  $D$  correlates with  $\nu_p$  and thus changes the shape of

the redshift-corrected  $\nu_p L_p$  versus  $\nu_p$  sequence, which has been considered in previous papers. We therefore checked how measurements of  $D_{var}$  from Hovatta et al. 2008 correlate with the  $D$ -corrected  $\nu_p$ . The Doppler correction of peak frequency was performed using equation

$$\nu'_p = \nu_p \left( \frac{1+z}{D_{var}} \right), \quad (3)$$

where the primed symbol represents the parameter value in the source rest frame. The result is presented in Fig. 1. The negative correlation is obvious, and the Spearman rank correlation test provides a correlation coefficient  $\rho = -0.698$  and a probability  $P < 0.001$  of no correlation. The correlation remains similar if we use values of  $\nu_p$  uncorrected for the Doppler factor. The sources with their synchrotron peak at low energies are significantly more boosted than high- $\nu_p$  sources. A similar negative correlation ( $\rho = -0.654$  and  $P = 0.004$ ) can be obtained using the Doppler factors of Jorstad et al. (2005), determined from variability data. We measured this also using the Doppler factors of Ghisellini et al. (1993), calculated from the difference between the observed X-ray flux and one predicted by synchrotron self-Compton theory, based on the observed VLBI data. In this case, the correlation is very strong ( $\rho = -0.517$  and  $P < 0.001$ ). Therefore, we conclude that dependence is similar irrespective of the method used to calculate the  $D$ -factors, and the negative correlation between  $D_{var}$  and  $\nu_p$  is robust.

Figure 1 also depicts the broadness of the range of  $D_{var}$ , stretching from close to 0 to 30. At low  $\nu_p$  in particular, it is crucial to have an accurate measurement of the source Doppler factor to obtain credible results of the intrinsic properties. Wu et al. (2007) determined Doppler factors derived from the relation between the observed 5 GHz core luminosity and a theoretical one, calculated from the total radio power at 408 MHz. Using  $\log \nu_p$ -values from Paper I, they also plotted the dependence between  $D$  and  $\nu_p$ . Their Fig. 13 bears a striking resemblance to Fig. 1 of this work.

### 4.2. $\nu_p L_p$ vs. $\nu_p$ -correlation

We examined the  $\nu_p L_p$  versus  $\nu_p$ -correlation using first redshift-corrected values and then Doppler-corrected, intrinsic values. We observe the results in Fig. 2. In the top panel, we display the observational,  $z$ -corrected correlation, and in the bottom panel the intrinsic,  $D$ -corrected correlation. The frequency redshift-correction is completed using the equation

$$\nu_{p,z} = \nu_p (1+z), \quad (4)$$

and the redshift-corrected luminosity  $L_{p,z}$  is calculated with the equation

$$L_{p,z} = \frac{4\pi d_L^2}{1+z} F_{\nu,p}, \quad (5)$$

where  $d_L$  denotes luminosity distance and  $F_{\nu,p}$  is determined from the SED. The Doppler-corrections are performed using Eq. 3 and the equation

$$L'_p = L_{p,z} \left( \frac{1+z}{D_{var}} \right)^{3+\alpha}, \quad \text{assuming } F \propto \nu^{-\alpha}. \quad (6)$$

In all equations, the subscript  $z$  represents redshift-corrected values and primed values are both redshift and Doppler-corrected. When using Eq. 6, we assumed a spectral index  $\alpha = 1$  according

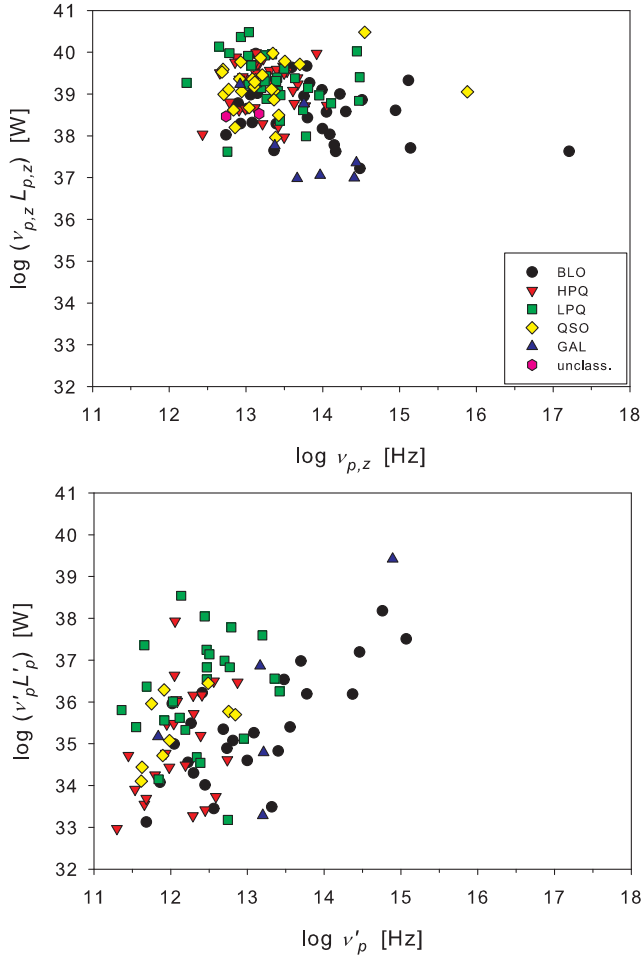


**Fig. 2.** The peak luminosity of the synchrotron component plotted versus the synchrotron peak frequency. In the top panel, the values are  $z$ -corrected, and in the bottom panel Doppler-corrected. AGN classes are marked with different symbols (see legend).

to the definition of the synchrotron peak of the SED. All equations concerning redshift- and Doppler-corrections can be found in e.g. Kembhavi & Narlikar (1999).

The blazar sequence is represented by a negative correlation between the synchrotron peak frequency  $\nu_p$  and peak luminosity  $\nu_p L_p$ . When our observational, redshift-corrected correlation is considered, we find that a significant correlation is also measured for our sample. The Spearman rank correlation test measures  $\rho = -0.248$  and  $P = 0.002$  for the entire sample. The Spearman test results for different AGN subclasses can be seen in Table 2: only the correlation of LPQs is found to be significant. Considering the entire sample, the trends visible in the top panel of Fig. 2 are similar to those of the blazar sequence scenario found in several previous papers.

The full sample of our study includes many sources that are not traditionally classified as blazars, although the blazar classification is not clearly defined. For consistency, we identified the bona fide blazars in our sample and measured the correlation for their data alone. We classified a source as a blazar if it is included in one of the following: i) the total blazar sample of Fossati et al. (1998), ii) the extragalactic radio sources list of Wall & Peacock (1985) and has  $\alpha_{2.75\text{ GHz}} \leq 0.5$  ( $S \propto \nu^{-\alpha}$ ), iii) the DXRBS

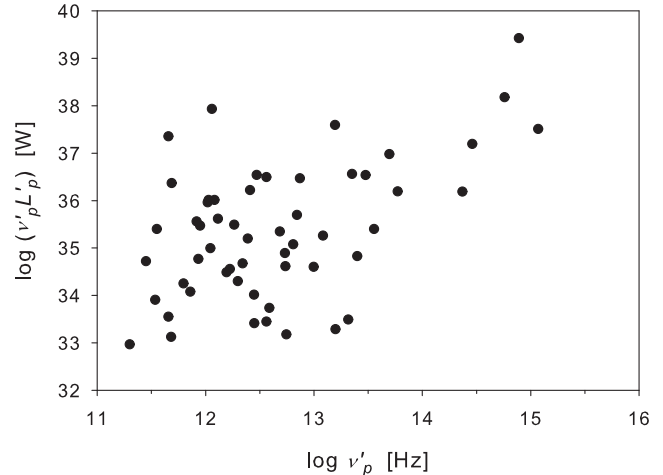


**Fig. 3.** The Doppler-corrected synchrotron peak luminosity vs. peak frequency correlation for bona fide blazars.

blazar sample of Perlman et al. (1998); or is classified as a BLO according to Table 1. There were 65 blazars that fulfilled at least one of these criteria, and they are marked in Col. (9) of Table 1. From Table 2, we observe that the blazar sequence can be found in our data when observational quantities are used, because there is a significant anticorrelation between the  $z$ -corrected  $\nu_p L_p$  and  $\nu_p$  for blazars alone. We list results also for the complete 1.2 Jy AGN subsample and separately for blazars belonging to the 1.2 Jy sample. For both subsets of data separately, the negative correlation is clearly significant.

We note that the observational anticorrelation detected here is not in disagreement with the conclusion of Paper I, which reported a lack of correlation between  $\nu_p L_p$  and  $\nu_p$  for BLOs. The range of  $\nu_p$  was very extended in Fig. 6 of that paper, whereas in Fig. 2 here the highest value of  $\log \nu_p$  is 17.2. When the range of  $\log \nu_p \leq 17$  alone is considered, the two figures become consistent. We note also that Paper I considered BLOs alone, and no redshift correction was applied to their data.

In the bottom panel of Fig. 2, we observe the effect of applying the Doppler-correction to the correlation. It is evident that the correlation is altered dramatically. For the entire sample, the results of the Spearman test are  $\rho = 0.353$  and  $P < 0.001$ , which implies that the correlation is *positive*. In Table 2, it is evident that, for BLOs, there is a remarkably clear positive correlation between  $\nu_p L_p$  and  $\nu_p$ . The correlations can be interpreted by comparison with Fig. 1. The sources of low  $\nu_p$  are more boosted, and their luminosity is lowered more significantly by the  $D$ -correction. For the blazar sample alone (Fig. 3), we also find a significant positive correlation ( $\rho = 0.366$  and  $P = 0.003$ ). Thus, we conclude that the blazar sequence, when defined as an anticorrelation of  $\nu_p L_p$  and  $\nu_p$ , is an artefact of variable Doppler boosting across the peak frequency range.

Interestingly, the positive correlation between the  $D$ -corrected  $\nu_p L_p$  and  $\nu_p$  for BL Lac objects can explain the peculiar U-shape in the  $\nu_p L_p$  versus  $\nu_p$  -correlation of Paper I (their Fig. 6). From Fig. 1, we deduce that for  $\log \nu_p \geq 15$ ,  $D_{var}$  is probably small, and the  $D$ -correction has little effect (see also Fig. 13 of Wu et al. (2007)). With this in mind, we considered datapoints with both  $\log \nu_p \geq 15$  and a measured redshift from Paper I, and applied a  $z$ -correction to the  $\nu_p$ -values. We then plotted these corrected data together with the  $D$ -corrected dat-

**Table 2.** Spearman rank correlation test results for the whole sample and AGN subclasses for the  $\log \nu_p L_p$  vs.  $\log \nu_p$  -correlation. On the left side is the  $z$ -corrected correlation, and on the right side the  $D$ -corrected one. Galaxies (GAL) have been omitted due to small sample size.

$z$ -corrected			$D$ -corrected		
Class	$\rho$	$P$	Class	$\rho$	$P$
All	-0.248	0.002	All	0.353	< 0.001
BLO	-0.220	0.126	BLO	0.642	< 0.001
HPQ	-0.049	0.390	HPQ	0.354	0.041
LPQ	-0.362	0.019	LPQ	0.236	0.128
QSO	0.110	0.296	QSO	0.550	0.063
Blazars	-0.329	0.004	Blazars	0.366	0.003
1.2 Jy AGN sample	-0.215	0.013	1.2 Jy AGN sample	0.340	0.002
1.2 Jy blazars	-0.287	0.020	1.2 Jy blazars	0.353	0.009

apoints for BLOs derived in this paper, producing the top panel of Fig. 4. After combining BLO data sets this way, we are able to observe an indisputable positive correlation ( $\rho = 0.637$  and  $P < 0.001$ ). It appears that the "intrinsic BLO sequence" implies that sources with higher  $\nu_p$  have higher  $\nu_p L_p$ ; this is completely the opposite conclusion to that of the original scenario. A similar trend was observed in two BLOs, 1101+384 (Mrk 421) and 1652+398 (Mrk 501), during flares (Pian et al. 1998; Takahashi et al. 2000). Their synchrotron peaks were shifted to higher frequencies by the luminosity increase triggered by the flare, in contrast to typical observations of the blazar sequence. For the case of 1652+398 in particular the shift was very pronounced. The positive correlation between peak frequency and luminosity is also in agreement with the number counts of low-energy BLOs (LBLs) and high-energy BLOs (HBLs), which indicate that HBLs are far less numerous than LBLs. As discussed in Padovani et al. (2007), this is difficult to understand if HBLs are intrinsically less luminous than LBLs.

As a cross-check, we plotted the BLO correlation using in addition the  $D^2$ -correction, that is the exponent  $2 + \alpha$  in Eq. 6 (bottom panel of Fig. 4). Both the content of the figure and the correlation coefficients of the combined BLO sequence changed only marginally. We also checked the  $D$ -corrected results of Table 2 using the  $D^2$ -correction. The significance of the positive correlations for the entire sample and the low- $\nu_p$  BLOs separately persists, while for HPQs, LPQs, and QSOS,  $P \geq 0.05$ . The main result of this paper, the disappearance of the blazar sequence with Doppler-correction, is therefore unchanged.

## 5. Discussion

As described in Paper I, the parabolic SED fit can overestimate the synchrotron peak frequency. This occurs in particular when the synchrotron peak occurs at or close to X-ray frequencies, when no datapoints constrain the parabolic fit beyond the X-ray domain. Here we have considered radio-bright quasars and blazars, whose peak frequencies are low; in this case, a parabolic fit is appropriate and negligible overestimation of the peak frequency occurs.

The intrinsic peak frequencies have been studied by Wu et al. (2007), who also found a significant negative correlation between  $D$  and  $\nu'_p$ . This independently corroborates the small Doppler factors of high-energy BLOs, and provides support to the concept of a BLO luminosity sequence presented in Fig. 4. After all, the  $\log \nu_p \geq 15$  -datapoints in their Fig. 13, for which  $D \leq 5$  approximately, are exactly the same ones, taken from Paper I, than those in the high- $\nu_p$  end of our Fig. 4. Wu et al. (2007) also measured a negative correlation between 408 MHz

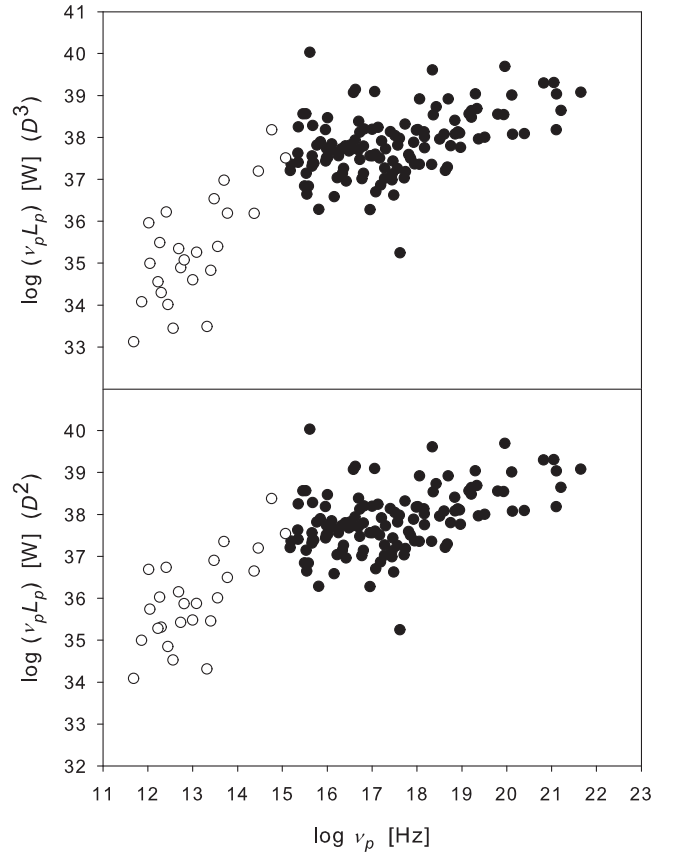


**Fig. 4.** Synchrotron peak luminosity versus peak frequency correlation for BLOs. The data are combined from this work (open circles) and Paper I (filled circles). The former are  $D$ -corrected, the latter are only  $z$ -corrected (i.e., we assume that they are not Doppler-boosted). In the top panel, the datapoints represented by open circles are  $D^3$ -corrected, in the bottom panel they are  $D^2$ -corrected. See text for details.

intrinsic luminosity and Doppler-corrected  $\nu_p$ . In our view this does not, however, correspond to a blazar sequence, which requires an anticorrelation between  $\nu_p$  and the luminosity at the synchrotron peak,  $\nu_p L_p$ , rather than for any particular frequency band. The correlation between radio luminosity and  $\nu_p$  can be generated by the shifting of the synchrotron parabola along the  $\log \nu$ -axis (from low-energy synchrotron source to high-energy synchrotron source), regardless of whether a genuine blazar sequence exists.

A strong positive correlation between  $\nu_p L_p$  and  $\nu_p$  for BLOs (Fig. 4) was unexpected. For these sources, the cooling effects may decrease and intrinsic luminosity increase as  $\nu_p$  increases. However, this phenomenon may not be restricted to BLOs: similar correlations may exist for other AGN classes. Unfortunately, to our knowledge there are no sufficiently large SED data sets that would allow us to investigate their respective luminosity sequences as extensively as that of BLOs. Looking at Table 2, we find that HPQs have a marginally significant positive intrinsic correlation, and QSOs are close to the limit. With more data-points for high values of  $\nu_p$  the correlation might also be significant for QSOs. LPQs, however, appear to differ from other classes, exhibiting no intrinsic correlation at all.

Another open question is the Compton dominance of low- $\nu_p$  sources. Fossati et al. (1998) and Ghisellini et al. (1998) found that as  $\nu_p$  decreased, the inverse Compton component became more luminous compared with its synchrotron counterpart in the SED. The accurate, observational determination of the shape and size of the Compton component for a large sample of objects would require a large amount of data from X-ray to TeV energies. Such a database is unfortunately not yet available for BLOs nor other AGN.

## 6. Conclusions

We have studied the correlation between the synchrotron peak frequency,  $\nu_p$ , and the synchrotron peak luminosity,  $\nu_p L_p$ , and the way that this changes when a Doppler-correction is applied to both quantities. We have used an extensive sample of 135 radio-bright AGN, a large part of which forms a complete flux-limited 1.2 Jy northern AGN sample. Our conclusions are as follows:

1. There is a clear negative correlation between the Doppler factor,  $D$ , and  $\nu_p$ , independent of the method for calculating  $D$ . This correlation has been tested using Doppler factors calculated from variability data, core versus extended flux, and synchrotron self-Compton flux. Typically, for sources with  $\log \nu_p \geq 15$ ,  $D$  is small, while low- $\nu_p$  sources may have values of  $D$  as high as 30 and thus be significantly boosted by comparison.
2. The negative correlation between  $\nu_p L_p$  and  $\nu_p$  at low  $\nu_p$ , known as the blazar sequence, is not present when the intrinsic, Doppler-corrected values are used. Instead, the correlation becomes *positive*. This is true for the entire AGN sample and a subsample of bona fide blazars. *The blazar sequence is an artefact of variable Doppler boosting across the peak frequency range.*
3. For BLOs in particular, there appears to be a strong intrinsic positive correlation between  $\nu_p L_p$  and  $\nu_p$ . This correlation is further strengthened when the BLO sample in this work is combined with the BLO sample of Nieppola et al. (2006). The positive correlation is also in accordance with number counts of LBLs and HBLs.

*Acknowledgements.* We gratefully acknowledge the funding from the Academy of Finland (project numbers 205793, 212656, and 210338). This research has made use of the NASA/IPAC Extragalactic Database (NED) which is operated by the Jet Propulsion Laboratory, California Institute of Technology, under contract with the National Aeronautics and Space Administration. E.N. thanks E.J. Lindfors for help with the high-energy data.

## References

Antón, S. & Browne, I. W. A. 2005, MNRAS, 356, 225

- Blandford, R. D. & Königl, A. 1979, ApJ, 232, 34  
 Caccianiga, A. & Marchã, M. J. M. 2004, MNRAS, 348, 937  
 Donato, D., Ghisellini, G., Tagliaferri, G., & Fossati, G. 2001, A&A, 375, 739  
 Fossati, G., Maraschi, L., Celotti, A., Comastri, A., & Ghisellini, G. 1998, MNRAS, 299, 433  
 Ghisellini, G., Celotti, A., Fossati, G., Maraschi, L., & Comastri, A. 1998, MNRAS, 301, 451  
 Ghisellini, G., Padovani, P., Celotti, A., & Maraschi, L. 1993, ApJ, 407, 65  
 Ghisellini, G. & Tavecchio, F. 2008, ArXiv e-prints, 0802.1918  
 Guerra, E. J. & Daly, R. A. 1997, ApJ, 491, 483  
 Güijosa, A. & Daly, R. A. 1996, ApJ, 461, 600  
 Jorstad, S. G., Marscher, A. P., Lister, M. L., et al. 2005, AJ, 130, 1418  
 Kembhavi, A. K. & Narlikar, J. V. 1999, Quasars and active galactic nuclei : an introduction (Quasars and active galactic nuclei : an introduction /Jit K. Kembhavi, Jayant V. Narlikar. Cambridge, U.K. : Cambridge University Press, c1999. ISBN 0521474779.)  
 Lähteenmäki, A. & Valtaoja, E. 1999, ApJ, 521, 493  
 Nieppola, E., Tornikoski, M., Lähteenmäki, A., et al. 2007, AJ, 133, 1947  
 Nieppola, E., Tornikoski, M., & Valtaoja, E. 2006, A&A, 445, 441  
 Padovani, P. 2007, Ap&SS, 309, 63  
 Padovani, P. & Giommi, P. 1995, ApJ, 444, 567  
 Padovani, P., Giommi, P., Ábrahám, P., Csizmadia, S., & Moór, A. 2006, A&A, 456, 131  
 Padovani, P., Giommi, P., Landt, H., & Perlman, E. S. 2007, ApJ, 662, 182  
 Padovani, P., Perlman, E. S., Landt, H., Giommi, P., & Perri, M. 2003, ApJ, 588, 128  
 Perlman, E. S., Padovani, P., Giommi, P., et al. 1998, AJ, 115, 1253  
 Pian, E., Vacanti, G., Tagliaferri, G., et al. 1998, ApJ, 492, L17+  
 Readhead, A. C. S. 1994, ApJ, 426, 51  
 Salonen, E., Teräsrananta, H., Urpo, S., et al. 1987, A&AS, 70, 409  
 Takahashi, T., Kataoka, J., Madejski, G., et al. 2000, ApJ, 542, L105  
 Teräsrananta, H., Achren, J., Hanski, M., et al. 2004, A&A, 427, 769  
 Teräsrananta, H., Tornikoski, M., Mujunen, A., et al. 1998, A&AS, 132, 305  
 Teräsrananta, H., Tornikoski, M., Valtaoja, E., et al. 1992, A&AS, 94, 121  
 Teräsrananta, H., Wiren, S., Koivisto, P., Saarinen, V., & Hovatta, T. 2005, A&A, 440, 409  
 Verkhodanov, O. V., Trushkin, S. A., Andernach, H., & Cherenkov, V. N. 2005, Bull. Special Astrophys. Obs., 58, 118  
 Véron-Cetty, M.-P. & Véron, P. 2000, A catalogue of quasars and active nuclei (A catalogue of quasars and active nuclei, 9th ed. Garching: European Southern Observatory (ESO), 2000, ESO Scientific Report no. 19.)  
 Wall, J. V. & Peacock, J. A. 1985, MNRAS, 216, 173  
 Wu, Z., Jiang, D. R., Gu, M., & Liu, Y. 2007, A&A, 466, 63

**Table 1.** The sample and the observational synchrotron peak frequencies obtained in this work. The values of  $\nu_p$  listed here have been determined directly from the SEDs and are not corrected for redshift nor for Doppler boosting.

Source	Alias	R.A.(J2000)	Dec(J2000)	1.2 Jy AGN sample	Class	$\log \nu_p$	$z$	Blazar sample
0003-066	NRAO 5	00:06:13.90	-06:23:35.34		BLO	12.80	0.347	*
0007+106	PG 0007+106	00:10:31.01	+10:58:29.50	*	GAL	13.34	0.089	
0014+813		00:17:08.47	+81:35:08.10	*	QSO	13.91	3.366	
0016+731		00:19:45.79	+73:27:30.02	*	LPQ	12.82	1.781	
0048-097	PKS 0048-097	00:50:41.32	-09:29:05.21		BLO	13.28	0.300	*
0059+581		01:02:45.76	+58:24:11.14	*	QSO	12.49	0.644	
0106+013	OC 012	01:08:38.77	+01:35:00.30		HPQ	12.73	2.107	
0109+224	S2 0109+22	01:12:05.80	+22:44:39.00	*	BLO	13.81		*
0133+476	DA 55	01:36:58.59	+47:51:29.10	*	HPQ	12.77	0.860	*
0149+218		01:52:18.06	+22:07:07.70	*	LPQ	13.04	1.320	
0202+149	4C 15.05	02:04:50.41	+15:14:11.00	*	HPQ	12.28	0.405	*
0212+735		02:17:30.81	+73:49:32.60	*	HPQ	12.34	2.367	*
0215+015		02:17:48.95	+01:44:49.70	*	HPQ	13.49	1.715	
0218+357	S4 0218+357	02:21:05.40	+35:56:15.00	*	QSO	12.75	0.936	
0219+428	3C 66A	02:22:39.60	+43:02:08.00	*	BLO	14.96	0.444	*
0224+671		02:28:50.05	+67:21:03.00	*	QSO	12.66	0.523	
0229+131		02:31:45.89	+13:22:54.72	*	LPQ	13.01	2.059	
0234+285	4C 28.07	02:37:52.41	+28:48:09.00	*	HPQ	12.81	1.207	
0235+164	AO 0235+164	02:38:38.80	+16:36:59.00	*	BLO	13.31	0.940	*
0248+430		02:51:34.54	+43:15:15.83	*	LPQ	13.45	1.311	
0300+470	4C 47.08	03:03:35.20	+47:16:17.00	*	BLO	14.34	0.475	*
0306+102	PKS 0306+102	03:09:03.60	+10:29:16.00	*	BLO	12.79	0.863	*
0316+413	3C 84	03:19:48.16	+41:30:42.10	*	GAL	14.40	0.017	*
0326+349		03:29:15.35	+35:10:08.10	*		12.99	0.500	
0333+321	NRAO 140	03:36:30.11	+32:18:29.30	*	LPQ	13.28	1.259	
0336-019	CTA 026	03:39:30.94	-01:46:36.00		HPQ	13.09	0.852	*
0355+508	NRAO 150	03:59:29.75	+50:57:50.20	*	QSO	12.53	1.510	
0415+379	3C 111	04:18:21.28	+38:01:35.80	*	GAL	13.64	0.049	
0420-014	OA 129	04:23:15.80	-01:20:33.10		HPQ	12.87	0.915	*
0422+004	OF 038	04:24:46.80	+00:36:07.00	*	BLO	14.83	0.310	*
0430+052	3C 120	04:33:11.10	+05:21:15.60	*	GAL	13.95 <sup>1</sup>	0.033	*
0440-003	NRAO 190	04:42:38.66	-00:17:43.00		HPQ	13.50	0.844	*
0446+112	PKS 0446+112	04:49:07.67	+11:21:28.00	*	GAL	12.58	1.207	
0454+039		04:56:47.10	+04:00:53.00		LPQ	14.11	1.343	
0458-020	PKS 0458-020	05:01:12.81	-01:59:14.00		HPQ	12.62	2.286	
0507+179		05:10:02.37	+18:00:41.58	*	QSO	12.71	0.416	
0528+134	PKS 0528+134	05:30:56.42	+13:31:55.15	*	LPQ	12.45	2.070	*
0552+398	DA 193	05:55:30.81	+39:48:49.17	*	LPQ	12.12	2.365	
0605-085	PKS 0605-085	06:07:59.70	-08:34:50.00		HPQ	13.40	0.872	*
0642+449	OH 471	06:46:32.03	+44:51:16.59	*	LPQ	12.39	3.406	
0716+714	S5 0716+714	07:21:53.30	+71:20:36.00	*	BLO	13.87	0.300	*
0723-008	PKS 0723-008	07:25:50.64	+00:54:56.54		GAL	14.39	0.127	
0735+178	PKS 0735+17	07:38:07.40	+17:42:19.00	*	BLO	14.07	0.424	*
0736+017		07:39:18.03	+01:37:04.60	*	HPQ	13.42	0.191	*
0738+313		07:41:10.70	+31:12:00.23	*	GAL	13.54	0.631	
0748+126		07:50:52.05	+12:31:04.83	*	LPQ	12.76	0.889	
0754+100	PKS 0754+100	07:57:06.64	+09:56:34.90	*	BLO	13.70	0.266	*
0804+499		08:08:39.67	+49:50:36.50	*	HPQ	12.75	1.430	
0814+425	OJ 425	08:18:16.00	+42:22:45.40	*	BLO	13.26	0.258	*
0823+033	PKS 0823+033	08:25:50.30	+03:09:24.00	*	HPQ	12.73	0.506	*
0827+243	OJ 248	08:30:52.08	+24:10:60.00	*	LPQ	12.94	0.941	
0829+046	PKS 0829+046	08:31:48.88	+04:29:39.09	*	BLO	13.92	0.180	*
0836+710	4C 71.07	08:41:24.37	+70:53:42.20	*	LPQ	13.94	2.170	*
0846+513		08:49:57.98	+51:08:29.00		QSO	13.24	1.860	
0850-1213		08:50:09.60	-12:13:34.00		QSO	12.58	0.566	
0851+202	OJ 287	08:54:48.80	+20:06:30.00	*	BLO	13.64	0.306	*
0906+430	3C 216	09:09:33.50	+42:53:46.08	*	HPQ	12.99	0.670	*
0917+449		09:20:58.46	+44:41:53.99	*	QSO	12.85	2.180	
0923+392	4C 39.25	09:27:03.01	+39:02:20.90	*	LPQ	11.99	0.699	*
0945+408	4C 40.24	09:48:55.34	+40:39:44.60	*	LPQ	12.87	1.252	

Table 1. continued.

Source	Alias	R.A.(J2000)	Dec(J2000)	1.2 Jy AGN sample	Class	$\log \nu_p$	$z$	Blazar sample
0953+254		09:56:49.88	+25:15:16.05	*	LPQ	13.03	0.712	
0954+556	S4 0954+556	09:57:38.24	+55:22:58.00	*	HPQ	13.77	0.901	*
0954+658	S4 0954+65	09:58:47.20	+65:33:54.00	*	BLO	14.16	0.367	*
1019+222		10:21:54.59	+21:59:31.20	*	GAL		1.617	
1036+054		10:38:46.78	+05:12:29.09	*		12.57	0.473	
1040+244	TEX 1040+244	10:43:09.00	+24:08:35.00	*	BLO	12.82	0.560	*
1039+811		10:44:23.06	+80:54:39.44	*	LPQ	13.04	1.260	
1049+215		10:51:48.79	+21:19:52.31	*	LPQ	12.84	1.300	
1055+018	OL 093	10:58:29.61	+01:33:58.80	*	HPQ	12.68	0.888	*
1150+812		11:53:12.50	+80:58:29.15	*	QSO	12.75	1.250	
1150+497		11:53:24.47	+49:31:08.83	*	HPQ	13.29	0.334	
1156+295	4C 29.45	11:59:31.83	+29:14:44.00	*	HPQ	13.44	0.729	
1219+285	ON 231	12:21:31.70	+28:13:58.00	*	BLO	15.10	0.102	*
1219+044		12:22:22.55	+04:13:15.78	*	QSO	13.07	0.965	
1222+216	PKS 1222+216	12:24:54.51	+21:22:47.00	*	QSO	13.27	0.435	
1226+023	3C 273	12:29:06.69	+02:03:08.60	*	LPQ	13.89	0.158	*
1253-055	3C 279	12:56:11.17	-05:47:21.50	*	HPQ	12.67	0.538	*
1308+326	AUCVn	13:10:28.66	+32:20:43.80	*	BLO	13.49	0.992	*
1324+224		13:27:00.86	+22:10:50.16	*	QSO	12.74	1.400	
1406-076	PKS 1406-076	14:08:56.48	-07:52:27.00	*	QSO	12.69	1.494	
1413+135	PKS 1413+135	14:15:58.80	+13:20:24.00	*	BLO	12.64	0.247	*
1418+546	OQ 530	14:19:46.60	+54:23:14.00	*	BLO	14.03	0.152	*
1502+106	OR 103	15:04:24.98	+10:29:39.00	*	HPQ	13.08	1.833	*
1510-089	PKS 1510-089	15:12:50.53	-09:05:59.00	*	HPQ	13.49	0.361	*
1532+016	PKS 1532+016	15:34:52.45	+01:31:04.00	*	HPQ	13.23	1.435	
1538+149	4C 14.60	15:40:46.50	+14:47:45.90	*	BLO	13.84	0.605	*
1546+027		15:49:29.44	+02:37:01.20	*	HPQ	12.97	0.413	
1548+056		15:50:35.27	+05:27:10.45	*	HPQ	12.74	1.422	
1606+106	4C 10.45	16:08:46.20	+10:29:07.80	*	LPQ	12.80	1.226	
1611+343	DA 406	16:13:41.00	+34:12:48.00	*	LPQ	12.69	1.401	*
1633+382	4C 38.41	16:35:15.49	+38:08:04.50	*	LPQ	12.89	1.814	*
1637+574	OS 562	16:38:13.46	+57:20:24.00	*	LPQ	13.17	0.745	*
1642+690		16:42:07.85	+68:56:39.76	*	HPQ	12.54	0.751	
1641+399	3C 345	16:42:58.81	+39:48:37.00	*	HPQ	12.71	0.595	*
1652+398	MRK 501	16:53:52.20	+39:45:36.00	*	BLO	17.19	0.034	*
1725+044	PKS 1725+044	17:28:24.95	+04:27:05.00	*	QSO	13.27	0.297	*
1730-130	NRAO 530	17:33:02.71	-13:04:49.55	*	QSO	12.42	0.902	
1739+522	S4 1739+52	17:40:36.98	+52:11:43.00	*	HPQ	12.93	1.379	
1741-038	PKS 1741-038	17:43:58.86	-03:50:04.60	*	HPQ	12.35	1.054	*
1749+096	PKS 1749+096	17:51:32.70	+09:39:01.00	*	BLO	12.78	0.320	*
1758+388		18:00:24.72	+38:48:31.10	*	QSO	12.70	2.092	
1803+784	S5 1803+784	18:00:45.40	+78:28:04.00	*	BLO	13.60	0.684	*
1807+698	3C 371	18:06:50.70	+69:49:28.00	*	BLO	14.46	0.051	*
1823+568	4C 56.27	18:24:07.07	+56:51:01.50	*	BLO	12.93	0.663	*
1828+487	3C 380	18:29:31.80	+48:44:46.62	*	LPQ	13.88	0.692	
1845+797	3C 390.3	18:42:08.99	+79:46:17.00	*	GAL		0.055	
1901+319		19:02:55.93	+31:59:41.70	*	QSO	15.67	0.635	
1926+61	S4 1926+61	19:27:30.40	+61:17:32.00	*	BLO	13.27		*
1928+738	4C 73.18	19:27:48.50	+73:58:01.60	*	LPQ	13.32	0.303	*
1954+513		19:55:42.74	+51:31:48.55	*	LPQ	12.90	1.223	
2007+776	S5 2007+77	20:05:31.10	+77:52:43.00	*	BLO	12.95	0.342	*
2005+403		20:07:44.94	+40:29:48.60	*	QSO	13.07	1.736	
2021+614	OW 637	20:22:06.68	+61:36:58.80	*	LPQ	12.67	0.227	*
2022+171		20:24:56.56	+17:18:13.20	*	LPQ	13.14	1.050	
2037+511		20:38:37.04	+51:19:12.66	*	QSO	12.26	1.687	
2059+034		21:01:38.83	+03:41:31.30	*	QSO	13.03	1.013	
2121+053		21:23:44.52	+05:35:22.09	*	HPQ	13.01	1.941	
2134+004	OX 057	21:36:38.59	+00:41:54.21	*	LPQ	12.32	1.936	*
2136+141		21:39:01.31	+14:23:36.00	*	LPQ	12.71	2.427	
2141+175		21:43:35.55	+17:43:48.50	*	LPQ	13.70	0.211	
2144+092		21:47:10.16	+09:29:46.67	*	QSO	13.04	1.113	

**Table 1.** continued.

Source	Alias	R.A.(J2000)	Dec(J2000)	1.2 Jy AGN sample	Class	$\log \nu_p$	$z$	Blazar sample
2145+067		21:48:05.46	+06:57:38.60	*	LPQ	12.73	0.990	*
2200+420	BL LAC	22:02:43.30	+42:16:39.00	*	BLO	14.14	0.070	*
2201+315	4C 31.63	22:03:14.98	+31:45:38.30	*	LPQ	13.63	0.298	
2201+171		22:03:26.89	+17:25:48.20	*	QSO	12.90	1.075	
2209+236	PKS 2209+236	22:12:05.97	+23:55:40.00	*	QSO	12.62	1.125	
2223-052	3C 446	22:25:47.30	-04:57:01.39		BLO	12.74	1.404	*
2227-088		22:29:40.09	-08:32:54.50		HPQ	12.99	1.562	
2230+114	CTA 102	22:32:36.41	+11:43:50.90	*	HPQ	13.19	1.037	*
2234+282		22:36:22.47	+28:28:57.41	*	HPQ	12.74	0.795	
2251+158	3C 454.3	22:53:57.75	+16:08:53.60	*	HPQ	12.83	0.859	*
2254+074	PKS 2254+074	22:57:17.30	+07:43:12.27		BLO	14.07	0.190	*
2344+092		23:46:36.84	+09:30:45.52	*	LPQ	14.25	0.677	*
2351+456	4C 45.51	23:54:21.68	+45:53:04.00	*	QSO	12.44	1.986	
2353+816		23:56:22.79	+81:52:52.26	*	QSO	12.74	1.344	

<sup>1</sup> =  $\log \nu_p$  determined from the highest flux density measurement of the synchrotron component of the SED (see Sect. 3.1).

# Online Material

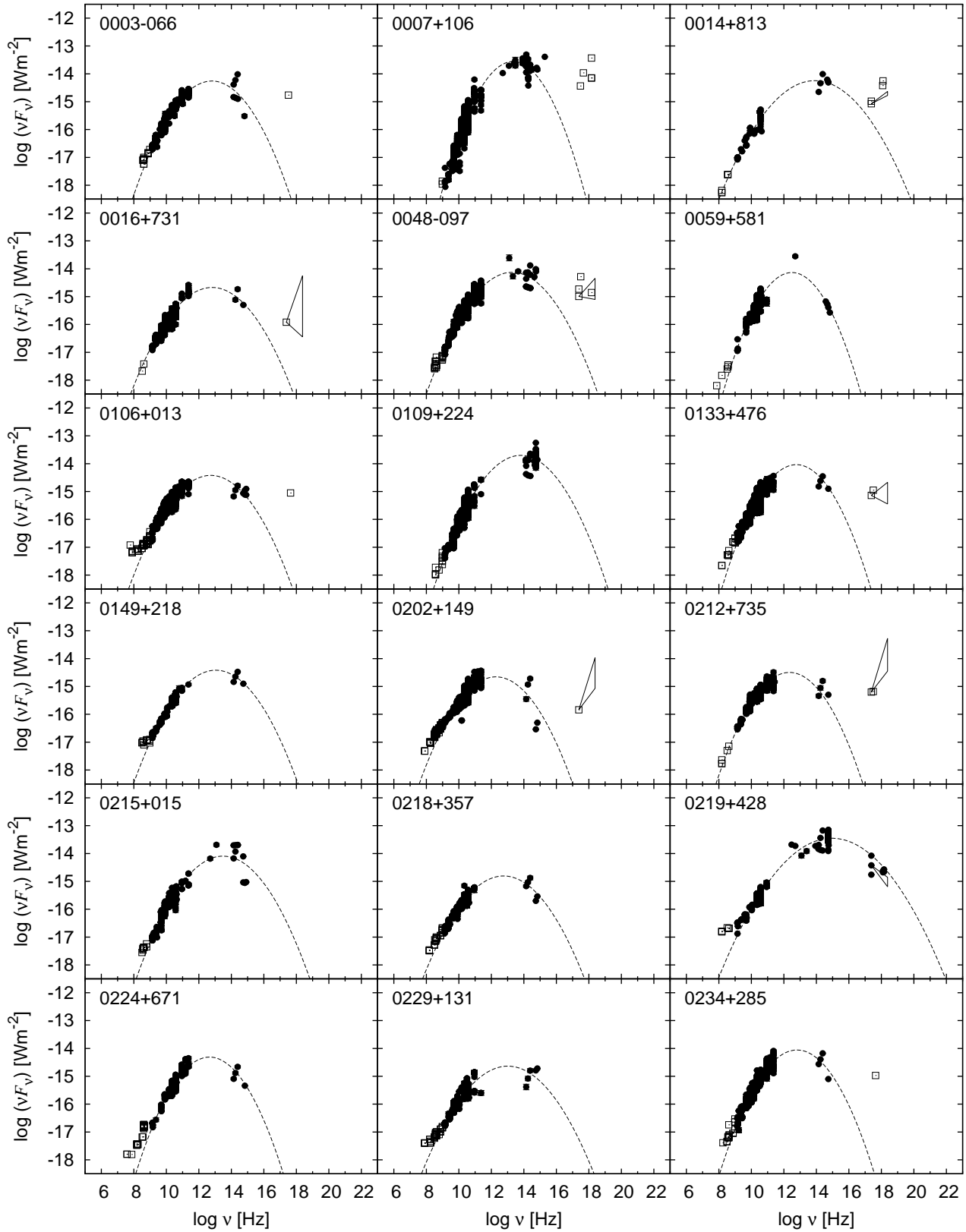


**Fig. 5.** The spectral energy distributions determined in this work. All quantities are observational and uncorrected for redshift and Doppler boosting. The dashed line represents the parabolic fit to the synchrotron component. Datapoints marked with filled circles are included in the fit, the empty squares are not. Sources 1019+222 and 1845+797 could not be fitted with a parabolic function.

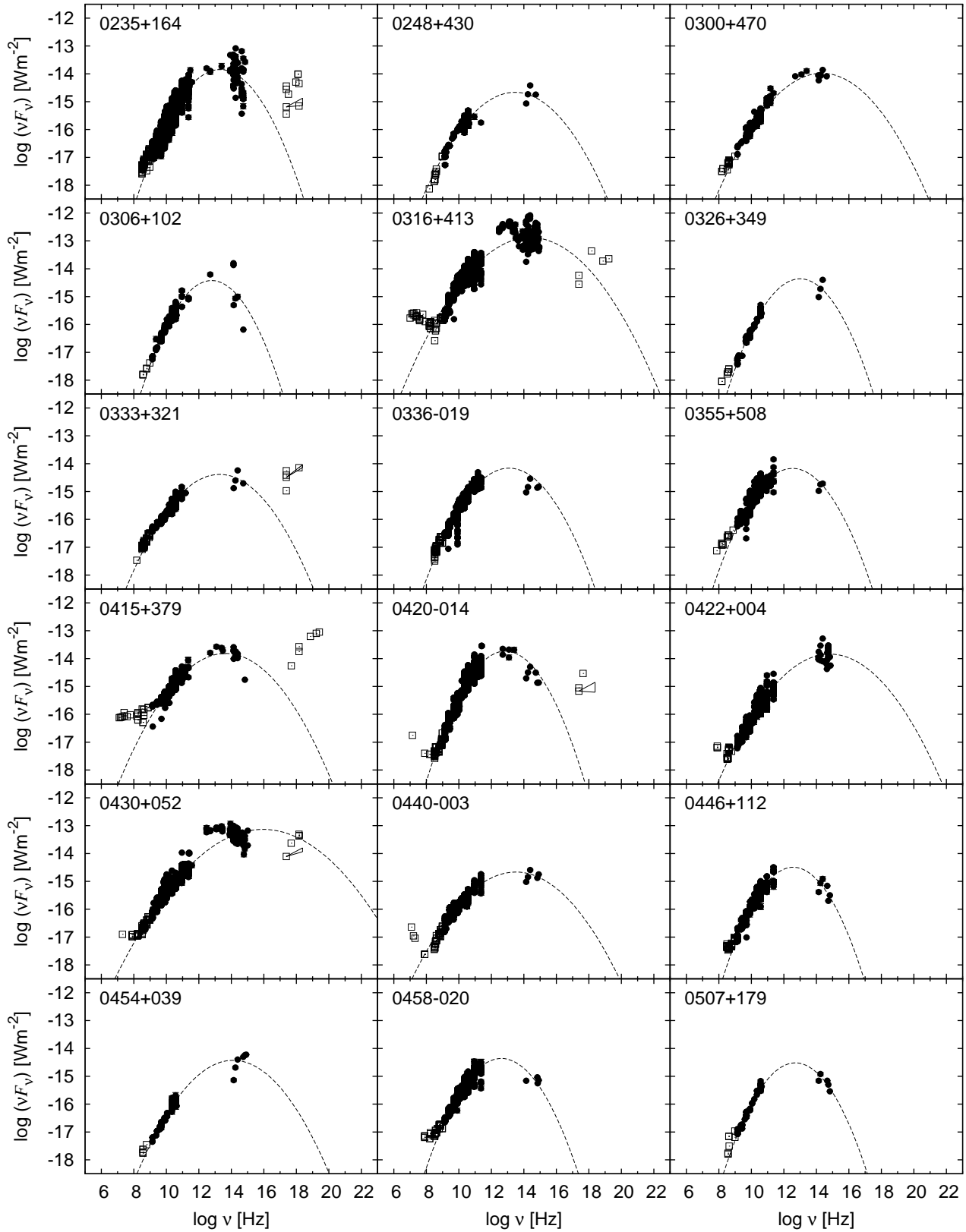


Fig. 5. continued.

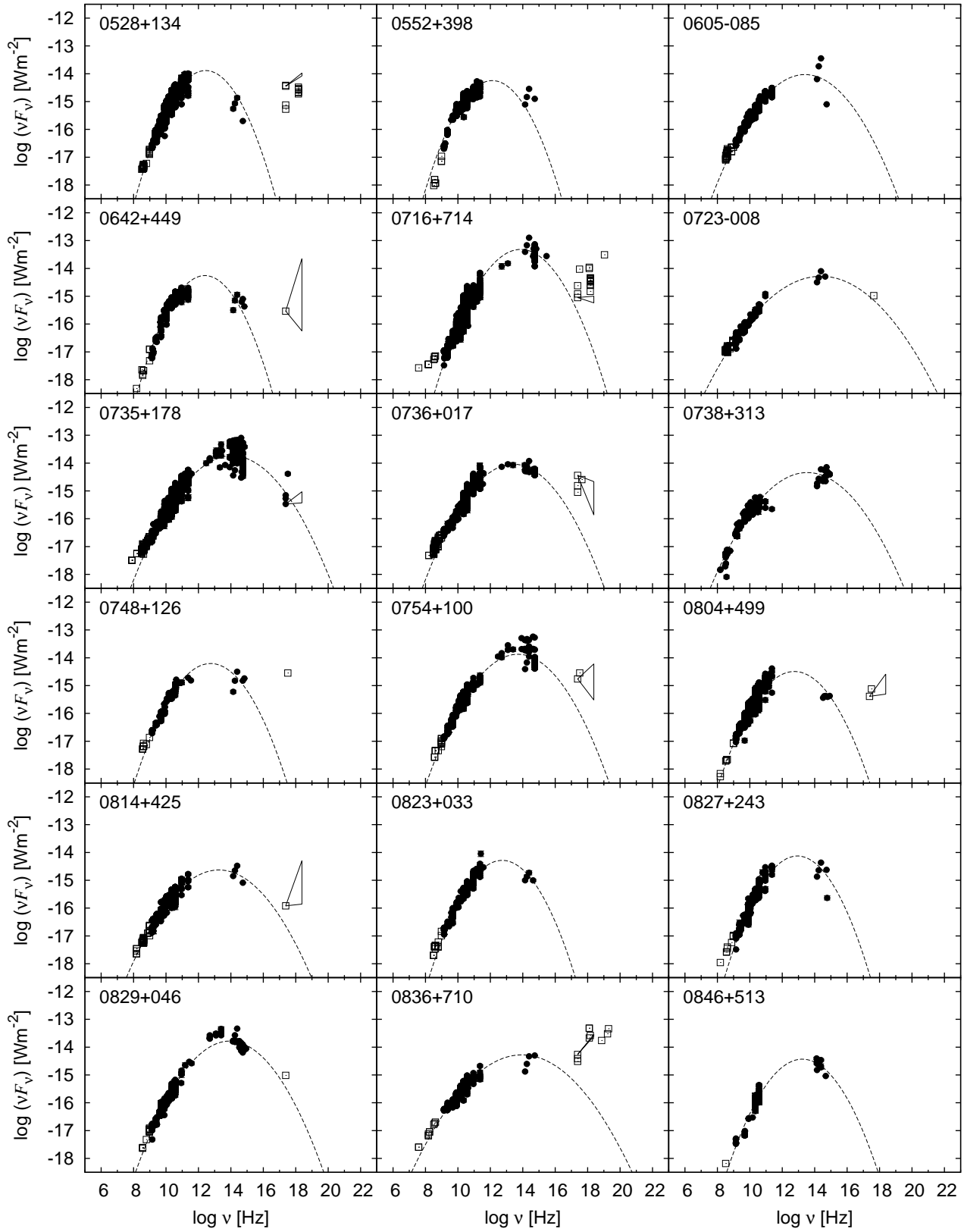


Fig. 5. continued.

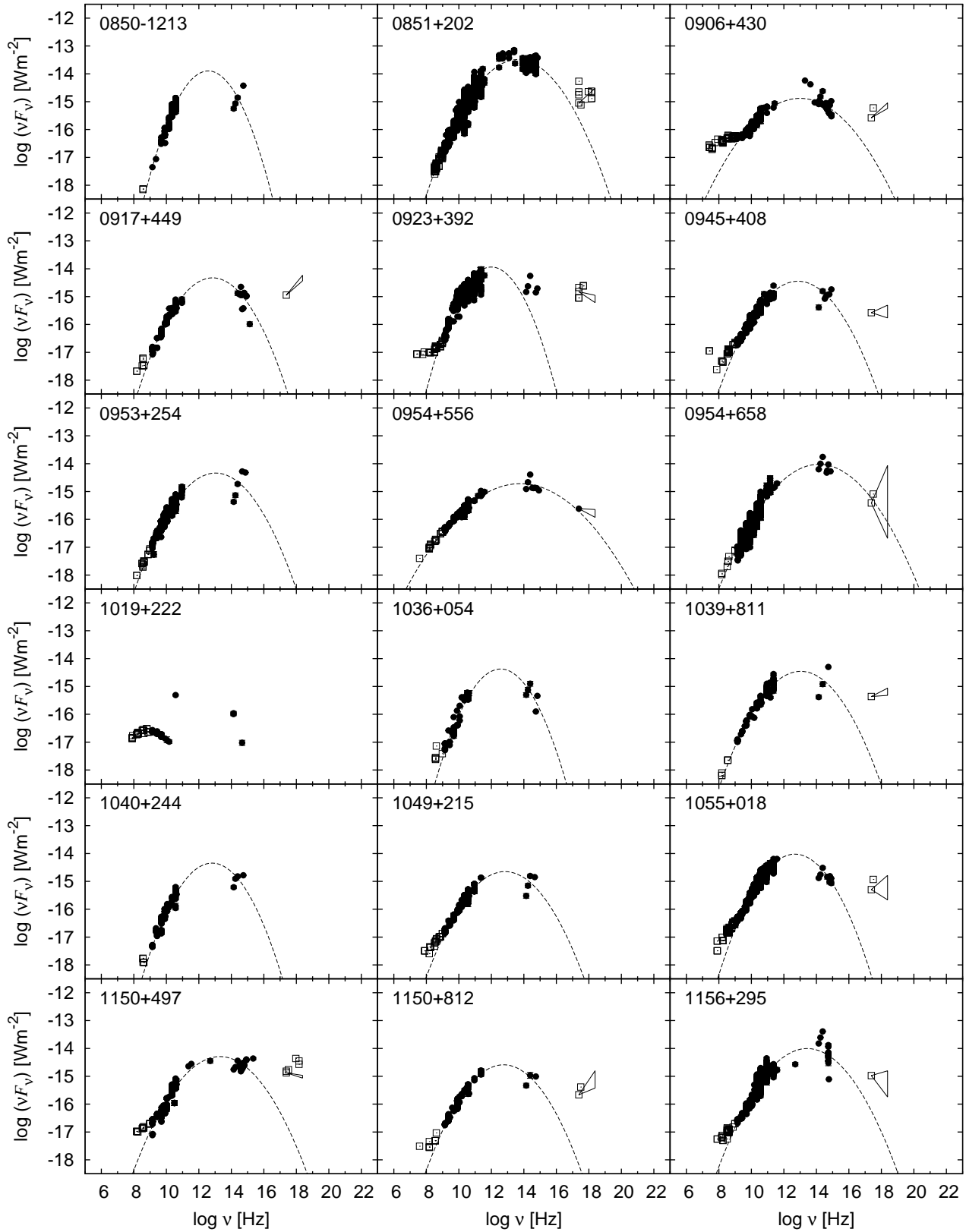


Fig. 5. continued.

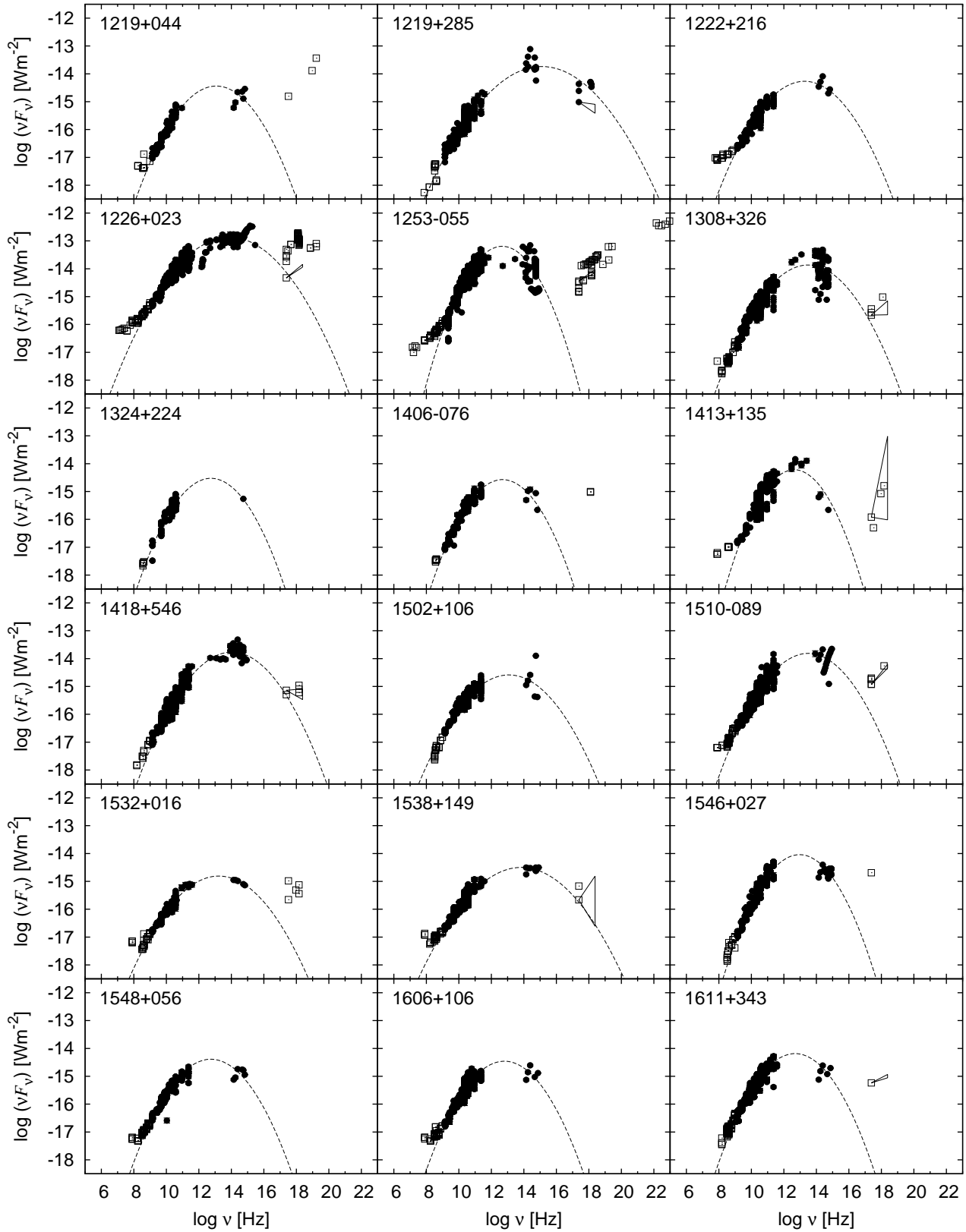


Fig. 5. continued.

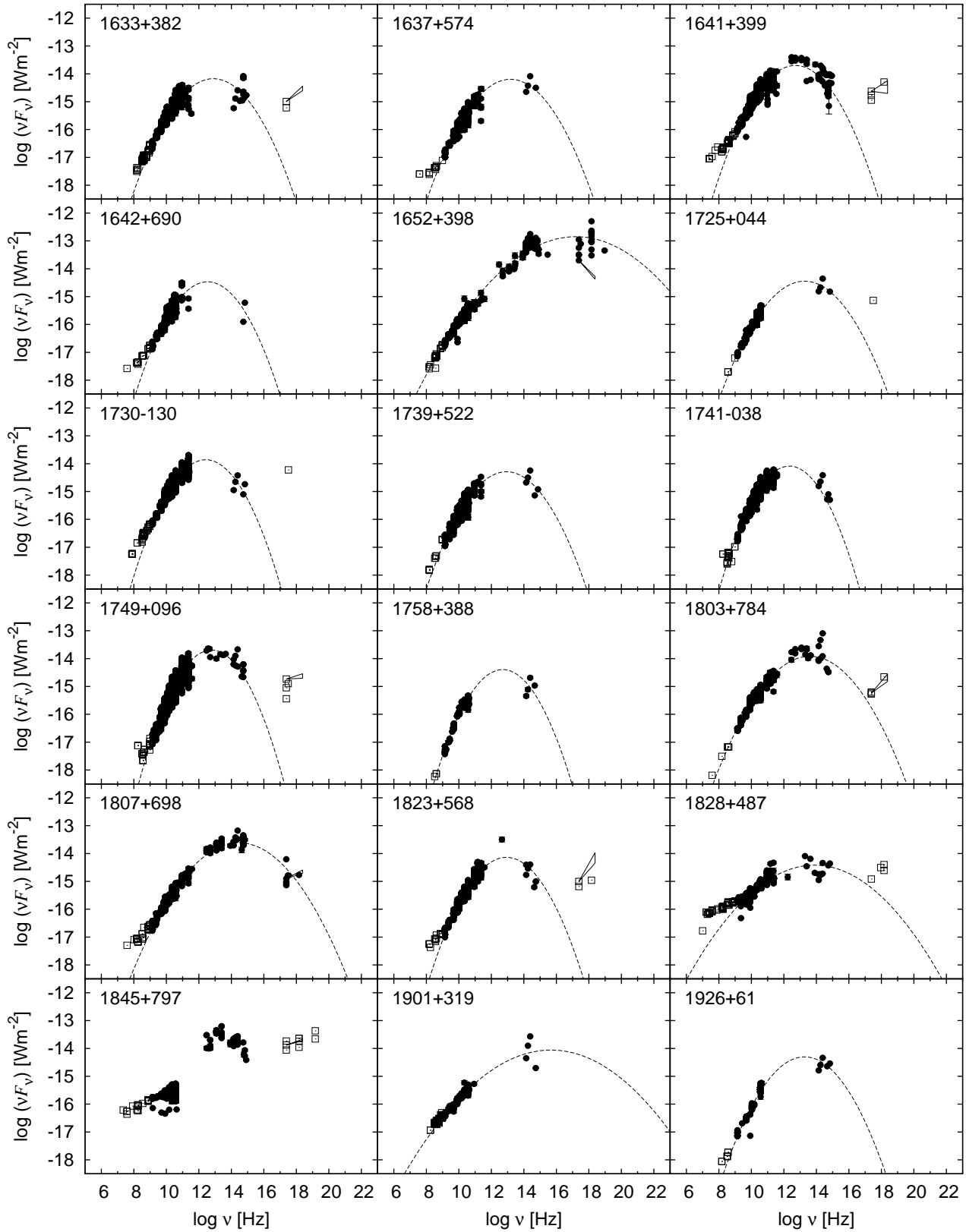


Fig. 5. continued.

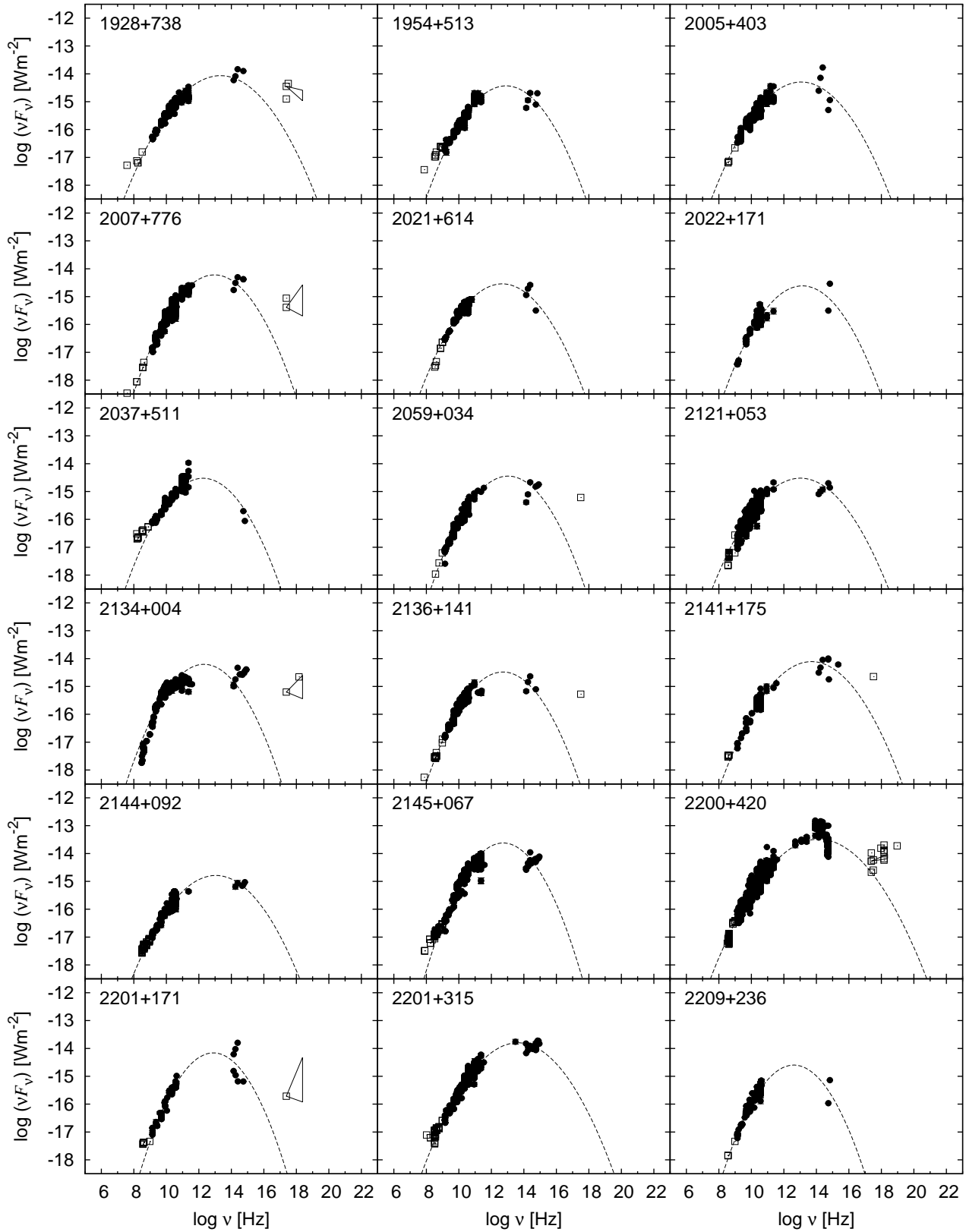


Fig. 5. continued.

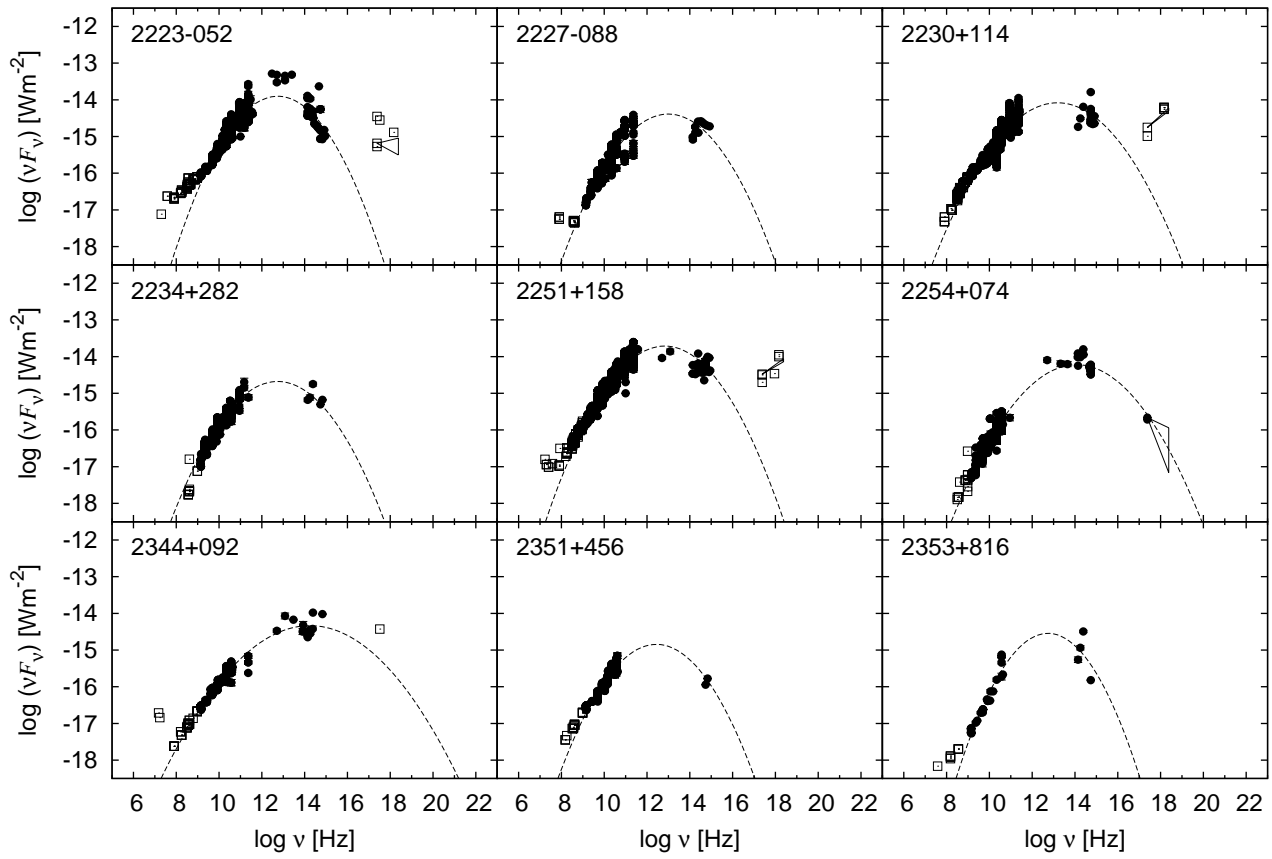


Fig. 5. continued.